Available online at www.sciencedirect.com
ScienceDirect
Cold Regions Science and Technology 47 (2007) 118–133
cold regions science and technology
www.elsevier.com/locate/coldregions

# Surface hoar characteristics derived from a snow micropenetrometer using moving window statistical operations

Eric Lutz [a,*], Karl W. Birkeland [a,b], Kalle Kronholm [a,c], Kathy Hansen [a], Richard Aspinall [d]

[a] Department of Earth Sciences, Montana State University, Bozeman, MT, USA
[b] USDA Forest Service National Avalanche Center, Bozeman, MT, USA
[c] International Centre for Geohazards, Norwegian Geotechnical Institute, Oslo, Norway
[d] Macaulay Institute, Aberdeen, UK

**Abstract**

This study aims to improve analytical techniques for studying stratigraphic dimensions and hardness characteristics of thin weak layers in the mountain snowpack, with particular interest to buried surface hoar layers. By determining which structural characteristics of such weak layers are associated with shear strength, we may be better able to monitor and predict stability, which is relevant for avalanche forecasting and management. We utilize moving window statistical operations to analyze SnowMicroPen (SMP) penetrometer hardness profiles of a buried surface hoar layer. Results indicate that significant weak layer thinning and hardening of the interface between the weak layer and its substratum coincided with significant increases in shear strength, as measured using a size-corrected shear strength index derived from concurrent stability tests. With aging, variations in slab thickness appeared to positively affect the hardness and inversely affect the coefficient of variation (CoV) of hardness of weak layer boundaries. These findings support previous research that proposed the strengthening of buried surface hoar layers results from the gradual penetration of the surface hoar crystals into the substratum which allows stronger bonds to form at this critical interface. These analytical techniques allow stratigraphic dimensions and hardness characteristics to be quantified and analyzed, improving our ability to monitor stratigraphic characteristics associated with shear strength and stability of the mountain snowpack.


*Keywords:* Snow microstructure; Snow stratigraphy; Snow hardness; Snow penetrometer; Persistent weak layer; Shear strength; Avalanches

## 1. Introduction

Researchers and avalanche forecasters have used a number of penetrometers over the years to analyze snow structure with the goal of better predicting avalanches (Bader et al., 1939; Bradley, 1968; Dowd and Brown, 1986; DeQuervain and Meister, 1987; Schneebeli and Johnson, 1998; Schweizer and Wiesinger, 2003; Mackenzie and Payten, 2002). Relationships between avalanche activity and generalized snowpack types derived from Ram profiles have been identified (DeQuervain and Meister, 1987) and used by avalanche forecasters (Schweizer and Wiesinger, 2003). Studies of the relationships between instabilities and thin weak layers, such as buried surface hoar, have been hindered by the spatial and force resolution of available penetrometers. With the advent of the SnowMicroPen (SMP), a high-resolution constant-speed penetrometer, hardness characteristics of thin

* Corresponding author. Tel.: +1 406 599 2107; fax: +1 406 994 6923.
*E-mail address:* elutz@montana.edu (E. Lutz).

0165-232X/$ - see front matter © 2006 Elsevier B.V. All rights reserved.
doi:10.1016/j.coldregions.2006.08.021

weak layers can now be more effectively quantified (Pielmeier and Schneebeli, 2003). This instrument has been successfully implemented to delineate stratigraphic and micro-mechanical characteristics of the mountain snowpack (Johnson and Schneebeli, 1999; Schneebeli, 1999; Schneebeli et al., 1999; Pielmeier et al., 2001; Kronholm et al., 2004).

In previous SMP-related research, weak layers such as buried surface hoar have been delineated as the segment of the raw resistance signal between the upper and lower transitions (Fig. 1a and d) (Birkeland et al., 2004). Using this technique, Birkeland et al. (2004) identified the microstructural hardness of buried surface hoar layers as a potential predictor of changes in shear strength. A temporal association was identified between the shear strength and the maximum penetration resistance of the weak layer, as recorded using the SMP. It was rationalized that the increase in maximum resistance demonstrates strengthening of the strongest bonds within the weak layer, which are critical to weak layer strength. Surprisingly, no change in weak layer thickness could be identified using this delineation method (Birkeland et al., 2004).

In this study we improve SMP analysis techniques for determining the stratigraphic dimensions and hardness characteristics of buried surface hoar weak layers by incorporating two fundamental concepts. First, we expanded the scope of study to include the upper and lower transitions of the apparent weak layer (circles 1 and 2 in Fig. 1a), since these segments represent the most probable locations where strengthening occurs between surface hoar crystals and adjacent strata (Davis et al., 1996, 1998; Jamieson and Schweizer, 2000). In this study, the dimension containing the apparent weak layer and the adjacent transitions is referred to as the separation distance (Fig. 1e).

Second, we employ moving window statistical operations to help identify stratigraphic changes in hardness characteristics. Stratigraphic locations within and adjacent to the weak layer can be identified by analyzing trends in overlapping segments of resistance profiles. Stratigraphic delineation of thin weak layers needs to account for the size of the sensor head. This is a situation where the scale of the sample support nears the scale of the natural phenomenon (Blöschl, 1999). While the depth of each resistance reading is measured at the tip of the sensor head, the resistance signal itself results from snow structures (and void spaces) contacting the sensor head (potentially) along its entire length. The length of the sensor head is evident in the resistance signal as transitions of approximately the same length as the sensor head, entering and exiting the weak layer (circles 1 and 2 in Fig. 1a). Since the sensor head is conical, one might expect the transition force to follow a quadratic function (Fig. 1b). However, since snow is a highly heterogonous material and layer boundaries may be gradual at this scale of measurement (e.g. millimeters long), the conical relationships are likely to be obscured (gray line in Fig. 1a).

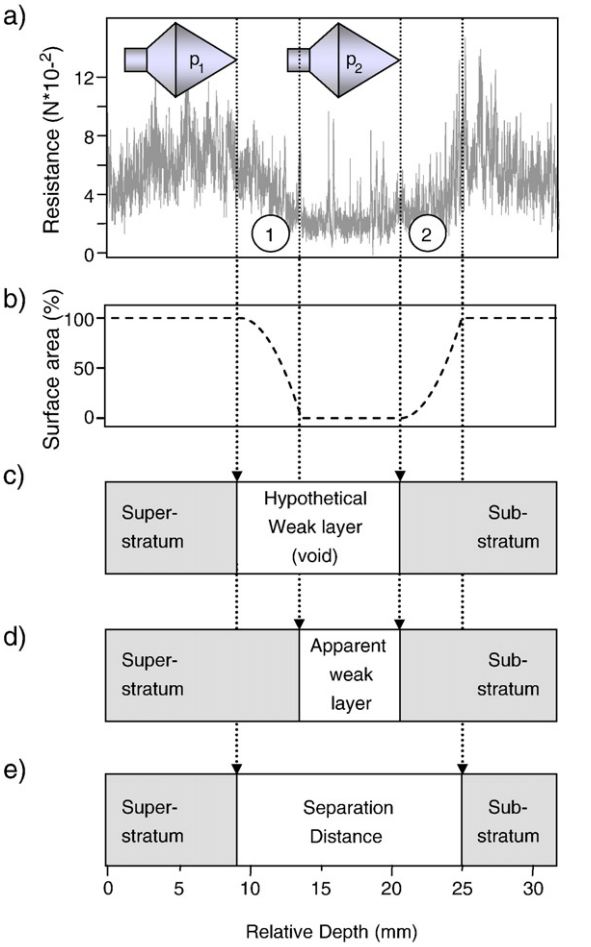


Fig. 1. (a) The SMP sensor head is depicted above a resistance profile of the weak layer of interest. The upper and lower transitions (circles 1 and 2) in the raw resistance values appear to be equal in length with the sensor head. The two superimposed sensor heads represent the probable location of the sensor head as it begins to enter ('$p_1$') and exit ('$p_2$') the weak layer. (b) The dotted line is an approximate descriptor of a hypothetical signal, representing a conical surface area function of the percentage of the sensor head that would be in contact with homogenous super- and substrata, assuming acute transition properties. The quadratically decreasing and increasing force values are less obvious in the raw force signal in (a), most likely due to heterogeneous nature of snow microstructure at the transitions. (c) The probable weak layer dimension based on (b). (d) Manual weak layer delineation, as conducted in previous research. (e) The separation distance examined in this study.

Using moving window statistical algorithms, we quantify stratigraphic dimensions and hardness variables which can then be examined for spatial and temporal patterns as well as potential associations with changes in shear strength. Since this study focused on improving our ability to analyze the SMP resistance signal and to identify potential associations with shear strength, the methodologies and results pay special attention to SMP signal processing and analysis techniques, while only briefly addressing the acquisition and analysis of the stability test data, which is extensively described by Landry et al. (2002).

## 2. Methods

### 2.1. Study site

The study site is located in southwestern Montana at the Lionhead area, a section of the Henry's Lake Mountains approximately 15 km west of West Yellowstone, Montana, USA (approximately 44°45′N; 111°15′W). The site is sheltered from ridge-top winds and maintains a northeast-facing aspect, both characteristics that are desirable for the development and preservation of surface hoar. Slope angles range between 25° and 28°, allowing for gravitational effects such as creep to occur, which may play an important role in snowpack evolution and avalanche formation (Louchet, 2001). Steeper slopes were not considered for safety reasons. The study site possesses relatively uniform substrate and vegetation characteristics, primarily sub-alpine grasses, forbs, and small shrubs.

### 2.2. Data acquisition

In order to assess the effectiveness of our methodologies, we analyzed data previously analyzed by Birkeland et al. (2004). Field data was collected in January 2002 (Landry et al., 2002; Birkeland et al., 2004). Slope-normal hardness profiles, stability tests, and a snow profile were conducted on January 9th and 15th at two adjacent plots, defined as plot 1 and plot 2, separated by approximately 100 m. All observations were registered on a local coordinate system, such that the *x*- and *y*-axes were cross- and up-slope axes, and the *z*-axis was slope-normal with origin at the snow surface (Fig. 2). The observations focused on monitoring the evolution of a buried surface hoar layer that had initially formed between December 21st and 26th and then was subsequently buried on December 27th. Weak layer thickness was estimated to the nearest centimeter, while the maximum surface hoar crystal size was estimated to the nearest millimeter.

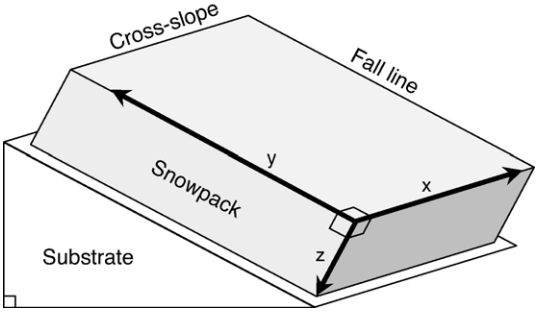


Fig. 2. The local coordinate system consisted of three axes: a slope-normal *z*-axis with origin at the snow surface was used to analyze slab and weak layer dimensions, a cross-slope *x*-axis and an up-slope *y*-axis.

Slope-normal hardness profiles were acquired using the SMP (Version 3.02). This penetrometer recorded approximately 180 resistance measurements per millimeter. The methodologies of SMP signal processing and analysis are described in the following sections.

The Quantified Loaded Column Test (QLCT) was utilized to measure *in situ* strength of the weak layer (Landry et al., 2001). Landry et al. (2001) have provided a detailed description of QLCT methodologies and Birkeland and Landry (2002) and Landry et al. (2004) have described this particular data set in detail.

Plot 1 was sampled on January 9th and contained 83 SMP profiles with a maximum sample spacing of 3 m and a minimum of 1 m (Fig. 3). Thirty QLCTs were performed at three pits embedded within the SMP sampling scheme; two additional pits from plot 1 were not regarded in this study since they were not surrounded by SMP measurements. Plot 2 was sampled on January 15th and contained 128 SMP profiles with a maximum point spacing of 3 m and a minimum of 0.5 m (Fig. 3). Forty-eight QLCTs were performed at five embedded pits. Although it was intended that both plots would possess the same spatial dimensions and sample sizes, mechanical difficulties hindered SMP data acquisition at plot 1. Although for an effective spatial comparison of SMP and QLCT data it would have been necessary to have QLCT tests distributed uniformly across both plots, pit-oriented tests were conducted for operational reasons and to enable pit-to-plot analysis during the original study (Landry et al., 2004).

### 2.3. SMP signal processing: moving window statistical operations

Using moving window statistical operations, several resistance variables, in the form of statistical profiles,

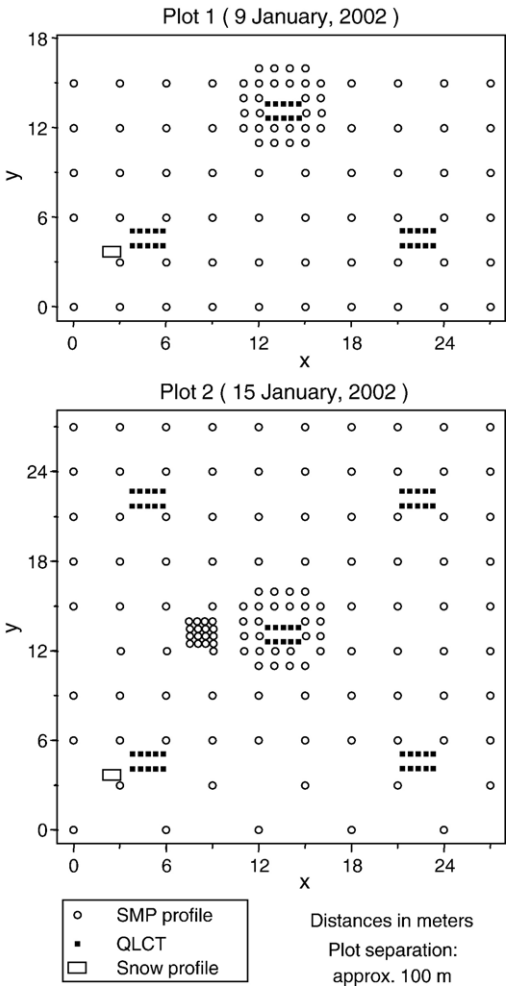


Fig. 3. Sample design at plots 1 and 2. The *x*-axis was oriented cross-slope and the *y*-axis up-slope.

were derived from the SMP measurements. The width of the moving window was equal to the length of the conical portion of the sensor head which, for this particular SMP, was 4.3 mm. This window length appeared to be a logical scale of aggregation for stratigraphic delineation and was confirmed in several trials using different window sizes. Smaller windows augmented tip interactions with individual crystals and caused stratigraphic boundaries to become less obvious while larger windows over-generalized hardness characteristics of the weak layer. On average, each window contained approximately 790 equally weighted resistance readings. While a general mechanical or probabilistic model could account for the conical shape of the sensor tip by incorporating weighted values that increase quadratically over the length of the window, by using an equal-weights window we made no

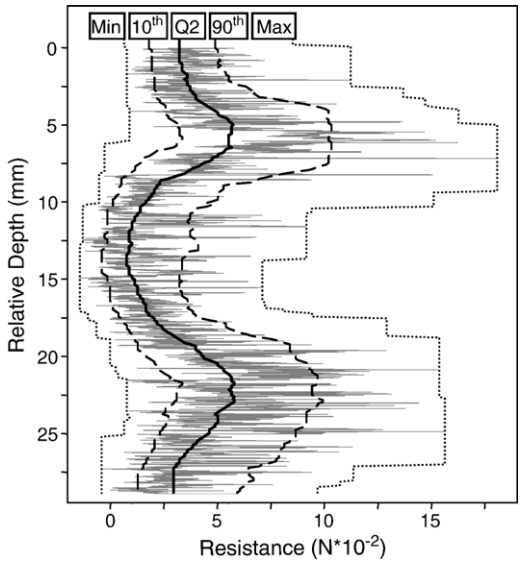


Fig. 4. Five of the statistical profiles generated from the SMP resistance signal (gray) at profile 10 in plot 2. These statistical profiles represent the minimum, the 10th percentile, the median (Q2), the 90th percentile and the maximum of the SMP signal encountered at the scale of the sensor head.

assumptions as to what part of the cone was in contact with structures at a given measurement.

The moving window spacing or offset was 0.1 mm (equal to approximately 20 measurements). Smaller

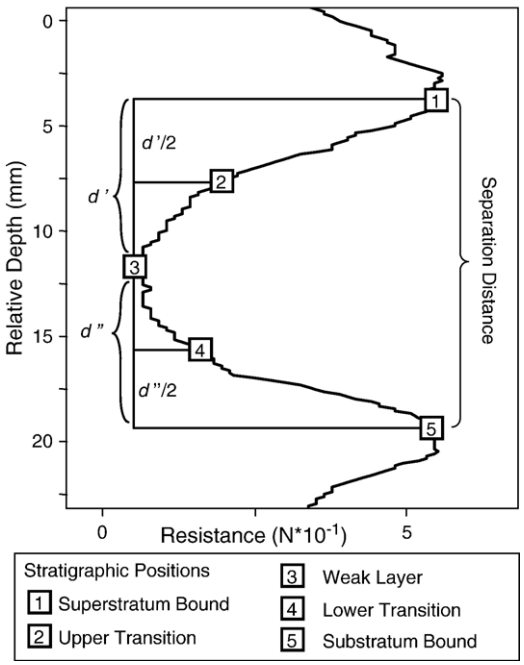


Fig. 5. The five defined stratigraphic positions within and adjacent to the weak layer are superimposed on a median profile from an SMP profile at plot 2.

Table 1
Spatial statistics of SMP-derived variables at plots 1 and 2

| Variable | Plot 1 (January 9th) | | | | | | | | | Plot 2 (January 15th) | | | | | | | | |
|---|---|---|---|---|---|---|---|---|---|---|---|---|---|---|---|---|---|---|
| | Best fit linear trend model | | | | Spherical semivariogram model | | | | | Best fit linear trend model | | | | Semivariogram model | | | | |
| | Sig. trend | Reg. type[a] | *p*-value | $R^2$ | Pos. auto-corr. | Range | Partial sill | Nugget | Nugget–sill | Sig. trend | Reg. type[a] | *p*-value | $R^2$ | Pos. auto-corr. | Range | Partial sill | Nugget | Nugget–sill |
| *Stratigraphic dimensions* | | | | | | | | | | | | | | | | | | |
| Slab thickness (mm) | Yes | 1 | 0.044 | 0.049 | No | – | – | – | – | Yes | 5 | 0.029 | 0.071 | Yes | 2.28 | 284.7414 | 96.3788 | 0.25 |
| Separation distance (mm) | Yes | 2 | 0.001 | 0.122 | Yes | 10.36 | 1.6662 | 4.2679 | 0.72 | No | 1 | 0.434 | 0.005 | No | – | – | – | – |
| Upper segment ($d'$) (mm) | No | 3 | 0.831 | 0.001 | No | – | – | – | – | No | 2 | 0.205 | 0.013 | No | – | – | – | – |
| Lower segment ($d''$) (mm) | Yes | 2 | 0.001 | 0.133 | No | – | – | – | – | No | 2 | 0.477 | 0.004 | No | – | – | – | – |
| *Superstratum boundary hardness* | | | | | | | | | | | | | | | | | | |
| Max ($N$) | No | 3 | 0.407 | 0.008 | No | – | – | – | – | Yes | 2 | 0.006 | 0.058 | Yes | 5.25 | 0.0007 | 0.0040 | 0.85 |
| 98th ($N$) | No | 2 | 0.289 | 0.014 | No | – | – | – | – | Yes | 2 | 0.003 | 0.068 | Yes | 1.81 | 0.0024 | 1.0e−10 | 4.1e−08 |
| 90th ($N$) | No | 2 | 0.215 | 0.019 | No | – | – | – | – | Yes | 2 | 0.003 | 0.066 | Yes | 1.45 | 0.0011 | 1.0e−10 | 9.3e−08 |
| 75th ($N$) | No | 2 | 0.264 | 0.015 | No | – | – | – | – | Yes | 2 | 0.003 | 0.069 | Yes | 2.27 | 0.0005 | 0.0002 | 0.32 |
| Median ($N$) | No | 2 | 0.286 | 0.014 | No | – | – | – | – | Yes | 2 | 0.003 | 0.067 | Yes | 5.92 | 0.0001 | 0.0004 | 0.73 |
| 25th ($N$) | No | 2 | 0.259 | 0.016 | No | – | – | – | – | Yes | 2 | 0.004 | 0.064 | Yes | 1.51 | 0.0004 | 1.0e−10 | 2.6e−07 |
| 10th ($N$) | No | 2 | 0.319 | 0.012 | No | – | – | – | – | Yes | 2 | 0.004 | 0.063 | Yes | 1.52 | 0.0003 | 1.0e−10 | 3.5e−07 |
| Min ($N$) | No | 2 | 0.469 | 0.006 | No | – | – | – | – | Yes | 5 | 0.001 | 0.124 | Yes | 1.54 | 0.0002 | 1.0e−10 | 6.5e−07 |
| CoV | No | 1 | 0.655 | 0.002 | No | – | – | – | – | No | 2 | 0.558 | 0.003 | Yes | 1.60 | 0.0046 | 1.0e−10 | 2.2e−08 |
| *Upper transition hardness* | | | | | | | | | | | | | | | | | | |
| Max ($N$) | No | 1 | 0.493 | 0.006 | Yes | 6.08 | 0.0034 | 0.0018 | 0.34 | Yes | 3 | 0.043 | 0.032 | No | – | – | – | – |
| 98th ($N$) | No | 1 | 0.868 | 0.000 | Yes | 7.50 | 0.0010 | 0.0013 | 0.55 | Yes | 5 | 0.037 | 0.066 | Yes | 1.71 | 0.0026 | 1.0e−10 | 3.8e−08 |
| 90th ($N$) | No | 1 | 0.695 | 0.002 | Yes | 2.36 | 0.0008 | 1.0e−10 | 1.2e−07 | No | 3 | 0.057 | 0.028 | Yes | 2.19 | 0.0007 | 0.0001 | 0.17 |
| 75th ($N$) | No | 1 | 0.581 | 0.004 | No | – | – | – | – | Yes | 2 | 0.015 | 0.046 | Yes | 4.01 | 0.0001 | 0.0002 | 0.63 |
| Median ($N$) | No | 1 | 0.697 | 0.002 | No | – | – | – | – | Yes | 3 | 0.007 | 0.056 | No | – | – | – | – |
| 25th ($N$) | No | 1 | 0.552 | 0.004 | No | – | – | – | – | Yes | 3 | 0.003 | 0.067 | Yes | 1.24 | 0.0001 | 1.0e−10 | 1.1e−06 |
| 10th ($N$) | No | 1 | 0.498 | 0.006 | No | – | – | – | – | Yes | 3 | 0.007 | 0.056 | No | – | – | – | – |
| Min ($N$) | Yes | 2 | 0.037 | 0.052 | Yes | 3.18 | 2.4e−05 | 2.4e−05 | 0.51 | Yes | 3 | 0.002 | 0.071 | No | – | – | – | – |
| CoV | No | 1 | 0.658 | 0.002 | No | – | – | – | – | No | 3 | 0.193 | 0.013 | Yes | 1.36 | 0.0284 | 0.0093 | 0.25 |

| | | | | | | | | | | | | | | | | | | |
|---|---|---|---|---|---|---|---|---|---|---|---|---|---|---|---|---|---|---|
| *Weak layer middle hardness* | | | | | | | | | | | | | | | | | | |
| Max (*N*) | No | 2 | 0.386 | 0.009 | Yes | 5.14 | 0.0033 | 0.0010 | 0.24 | Yes | 2 | 0.023 | 0.040 | No | – | – | – | – |
| 98th (*N*) | No | 2 | 0.680 | 0.002 | Yes | 5.05 | 0.0010 | 0.0009 | 0.47 | Yes | 3 | 0.019 | 0.043 | No | – | – | – | – |
| 90th (*N*) | No | 5 | 0.470 | 0.031 | No | – | – | – | – | Yes | 3 | 0.001 | 0.084 | No | – | – | – | – |
| 75th (*N*) | No | 5 | 0.398 | 0.037 | No | – | – | – | – | Yes | 3 | 3.6e−04 | 0.097 | No | – | – | – | – |
| Median (*N*) | No | 5 | 0.411 | 0.036 | No | – | – | – | – | Yes | 3 | 3.1e−04 | 0.098 | No | – | – | – | – |
| 25th (*N*) | No | 5 | 0.525 | 0.028 | No | – | – | – | – | Yes | 3 | 2.9e−04 | 0.099 | No | – | – | – | – |
| 10th (*N*) | No | 5 | 0.424 | 0.035 | No | – | – | – | – | Yes | 3 | 8.6e−05 | 0.116 | No | – | – | – | – |
| Min (*N*) | No | 1 | 0.370 | 0.010 | No | – | – | – | – | Yes | 2 | 5.1e−06 | 0.153 | Yes | 6.77 | 2.2e−05 | 2.7e−05 | 0.56 |
| CoV | No | 5 | 0.285 | 0.047 | No | – | – | – | – | Yes | 3 | 0.005 | 0.062 | No | – | – | – | – |
| *Lower transition hardness* | | | | | | | | | | | | | | | | | | |
| Max (*N*) | No | 1 | 0.197 | 0.020 | Yes | 7.59 | 0.0017 | 0.0008 | 0.32 | Yes | 2 | 0.026 | 0.039 | No | – | – | – | – |
| 98th (*N*) | No | 1 | 0.086 | 0.036 | Yes | 6.75 | 0.0014 | 0.0003 | 0.19 | Yes | 3 | 0.008 | 0.054 | Yes | 8.54 | 0.0004 | 0.0012 | 0.77 |
| 90th (*N*) | No | 1 | 0.077 | 0.038 | Yes | 6.85 | 0.0010 | 0.0002 | 0.18 | Yes | 3 | 0.011 | 0.050 | Yes | 8.28 | 0.0003 | 0.0006 | 0.68 |
| 75th (*N*) | No | 1 | 0.104 | 0.032 | Yes | 6.78 | 0.0006 | 0.0002 | 0.29 | Yes | 3 | 0.009 | 0.053 | Yes | 5.29 | 0.0003 | 0.0003 | 0.53 |
| Median (*N*) | No | 1 | 0.137 | 0.027 | No | – | – | – | – | Yes | 3 | 0.004 | 0.065 | Yes | 4.47 | 0.0002 | 0.0001 | 0.30 |
| 25th (*N*) | No | 1 | 0.227 | 0.018 | Yes | 5.94 | 0.0001 | 0.0001 | 0.58 | Yes | 3 | 0.001 | 0.086 | Yes | 7.76 | 0.0007 | 0.0003 | 0.28 |
| 10th (*N*) | No | 2 | 0.260 | 0.016 | No | – | – | – | – | Yes | 3 | 3.4e−05 | 0.128 | No | – | – | – | – |
| Min (*N*) | Yes | 2 | 0.025 | 0.060 | No | – | – | – | – | Yes | 3 | 1.7e−06 | 0.167 | Yes | 12.47 | 2.1e−05 | 3.4e−05 | 0.61 |
| CoV | No | 5 | 0.225 | 0.053 | No | – | – | – | – | Yes | 3 | 0.001 | 0.080 | Yes | 1.52 | 0.0175 | 0.0009 | 0.05 |
| *Substratum boundary hardness* | | | | | | | | | | | | | | | | | | |
| Max (*N*) | Yes | 1 | 0.010 | 0.079 | Yes | 6.08 | 0.0034 | 0.0018 | 0.34 | Yes | 5 | 0.017 | 0.079 | Yes | 8.12 | 0.0027 | 0.0023 | 0.47 |
| 98th (*N*) | Yes | 1 | 0.010 | 0.080 | Yes | 6.39 | 0.0037 | 1.0e−10 | 2.7e−08 | Yes | 5 | 0.005 | 0.099 | Yes | 7.96 | 0.0022 | 0.0011 | 0.33 |
| 90th (*N*) | Yes | 1 | 0.012 | 0.076 | Yes | 6.94 | 0.0032 | 1.0e−10 | 3.1e−08 | Yes | 5 | 0.001 | 0.121 | Yes | 7.93 | 0.0016 | 0.0007 | 0.31 |
| 75th (*N*) | Yes | 1 | 0.013 | 0.074 | Yes | 6.92 | 0.0027 | 1.0e−10 | 3.7e−08 | Yes | 5 | 0.001 | 0.124 | Yes | 8.08 | 0.0014 | 0.0006 | 0.29 |
| Median (*N*) | Yes | 1 | 0.015 | 0.070 | Yes | 6.94 | 0.0022 | 1.0e−10 | 4.6e−08 | Yes | 5 | 0.001 | 0.128 | Yes | 7.87 | 0.0011 | 0.0003 | 0.22 |
| 25th (*N*) | Yes | 4 | 0.022 | 0.091 | Yes | 7.05 | 0.0017 | 1.0e−10 | 5.9e−08 | Yes | 5 | 0.001 | 0.124 | Yes | 4.15 | 4.2e−05 | 1.9e−05 | 0.31 |
| 10th (*N*) | Yes | 5 | 0.010 | 0.133 | Yes | 6.98 | 0.0013 | 1.0e−10 | 7.8e−08 | Yes | 5 | 0.001 | 0.121 | Yes | 7.84 | 0.0005 | 0.0002 | 0.32 |
| Min (*N*) | Yes | 2 | 0.004 | 0.097 | Yes | 6.67 | 0.0006 | 1.0e−10 | 1.6e−07 | Yes | 5 | 0.001 | 0.131 | Yes | 7.89 | 0.0003 | 0.0001 | 0.28 |
| CoV | Yes | 5 | 0.002 | 0.171 | Yes | 5.56 | 0.0013 | 0.0009 | 0.42 | Yes | 5 | 0.007 | 0.093 | Yes | 5.72 | 0.0022 | 0.0016 | 0.43 |

For each variable, the best fit trend surface is listed with *p*- and $R^2$-values. Variables possessing positive spatial autocorrelation have spherical semivariogram dimensions listed. Reg. type indicates which linear model, as defined in the footnote of this table, offered the best fit; Sig. trend signifies the presence or absence of a significant ($p \leq 0.05$) linear trend, while Pos. auto-corr. signifies the presence or absence of positive spatial autocorrelation. For both trend- and semivariance analyses, $n_{plot1}=83$, $n_{plot2}=128$.

[a] Regression models: 1: $t(s) \sim x$; 2: $t(s) \sim y$; 3: $t(s) \sim x{:}y$; 4: $t(s) \sim x+y$; 5: $t(s) \sim x+y+x{:}y$, whereby '$t(s)$' denotes the trend surface, '$x$' and '$y$' the cross- and up-slope coordinates, and '$x{:}y$' the relationship between $x$ and $y$.

offsets would have unnecessarily increased data redundancy. One-dimensional semivariance analysis on several segments of multiple SMP profiles revealed that the signal typically possessed strong autocorrelation to distances of up to 0.08 mm (0.1 mm rounded to the nearest tenth of a millimeter). In this study this dimension was considered a good estimate of the dimension at which data redundancy occurred, although this dimension can also be useful for microstructural studies that focus on individual bond characteristics of snow types (Pielmeier and Schneebeli, 2000).

Using the above defined moving window dimensions, 9 statistical profiles were created from each SMP profile, including the minimum and maximum, the 10th-, 25th-, 50th-, 75th-, 90th-, and 98th percentiles, and the coefficient of variation (CoV) of the resistance signal, which is the ratio of the standard deviation to the mean. The non-parametric descriptors were utilized since the SMP signal is generally non-normally distributed (skewed toward lower values with outliers at higher values). Fig. 4 depicts five of the nine statistical profiles for the weak layer segment of a single SMP profile. It is important to understand that each position in a statistical profile represents a statistical value that was derived from an equal-weighted section of SMP signal the length of the sensor head.

### 2.4. Defining slope-normal stratigraphic positions and dimensions

The snow surface was identified in each SMP profile and was defined as the reference position (0 mm) on the slope-normal axis of the plot coordinate system ($z$-axis in Fig. 2). Five slope-normal stratigraphic positions were defined within and adjacent to the weak layer. This was done by locating three stratigraphic characteristics consistently evident in all of the median profiles at both plots. First, the minimum value of the median profile was defined as the center of the weak layer (Figs. 4 and 5). When multiple positions within the weak layer possessed the minimum value, then their median position was defined as the center of the weak layer. Second, two adjacent maximums at the apparent boundaries with adjacent strata (i.e. where the super- and substrata begin to subside into the weak layer) were defined as the superstratum and substratum boundaries (Figs. 4 and 5). Third, two additional positions were defined between the weak layer center and the apparent boundaries and are referred to as the upper and lower transitions (Fig. 5).

The slope-normal dimensions of the slab and the weak layer were calculated at each SMP profile. The slab thickness was defined as the distance from the snow surface to the superstratum boundary. The separation distance, a measure related to weak layer thickness, was defined as the distance between the superstratum and substratum boundaries (Fig. 5). The upper and lower segments of the separation distance were defined as the distances from the weak layer minimum to the adjacent boundaries ($d'$ and $d''$ in Fig. 5).

### 2.5. Statistical analysis

For each SMP profile, all 9 statistical profiles were sampled at the five above-defined stratigraphic positions within and adjacent to the weak layer. Hence, five sets of hardness information were generated from the statistical profiles for the five slope-normal stratigraphic positions within or adjacent to the weak layer (Fig. 5).

Spatial analysis was conducted to identify, at plot 1 or plot 2, significant spatial patterns in the SMP-derived stratigraphic dimensions and hardness variables. All SMP-derived variables were tested for two components of spatial structure, including spatial trends and positive spatial autocorrelation. In addition to the description provided here, Fotheringham et al. (2002) and O'Sullivan and Unwin (2002) provide overviews and Cressie (1993) describes spatial analysis techniques thoroughly.

For each SMP-derived variable, five trend surfaces $t(s)_{1-5}$ were calculated using five linear regressions models,

$$t(s)_1 = \alpha x + c_t$$

$$t(s)_2 = \beta y + c_t$$

$$t(s)_3 = \alpha x + \beta y + c_t$$

$$t(s)_4 = \alpha x : \beta y + c_t$$

$$t(s)_5 = \alpha x + \beta y + \alpha x : \beta y + c_t$$

whereby $\alpha$, $\beta$, and $c_t$ are regression coefficients, $x$ and $y$ are the cross- and up-slope SMP measurement coordinates (Fig. 3), and ':' signifies the relationship between $x$ and $y$. For each variable, the regression model with greatest significance was chosen as the best fit trend surface model. When no significant ($p \leq 0.05$) trend existed for a given variable, the mean of the variable was considered its best fit trend surface model.

SMP-derived variables were then tested for positive spatial autocorrelation by conducting semivariance analysis on the residuals of the best fit trend surface models. When positive spatial autocorrelation was evident in a semivariogram (i.e. semivariance increased with lag distance, until a sill threshold value was reached) then

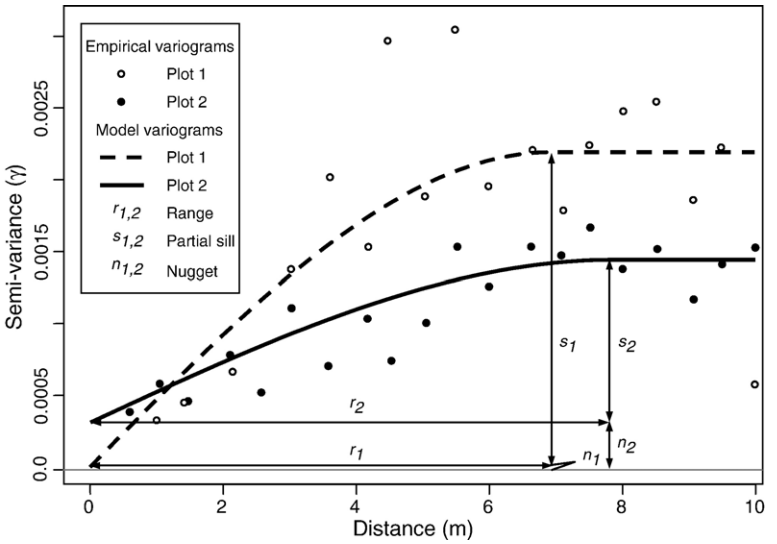


Fig. 6. Empirical and spherical modeled semivariograms of the median hardness of the substratum boundary at plots 1 and 2 (semivariance analysis utilized the following sample sizes: $n_{plot1}=83$, $n_{plot2}=128$). Between plots 1 and 2, the changes in model dimensions (increase in range, decrease in partial sill and increase in nugget) were evident in nearly all hardness variables at the substratum boundary.

spherical semivariogram models were fitted to empirical semivariograms using a weighted least squares function (Cressie, 1993, p. 97). The modeled semivariogram dimensions, including the range, partial sill, nugget, and nugget–sill ratio were recorded.

Classical statistical analysis was performed. Between plots 1 and 2, significant changes in SMP-derived variables were identified using the non-parametric Mann–Whitney (Wilcoxon Rank-Sum) test; boxplots were also used to graphically identify outliers and differences in central tendency. At each plot, spatially inherent relationships between slab thickness and weak layer characteristics (hardness and thickness) were tested for and quantified using simple linear regression. For this analysis, uncorrected SMP-derived variables were tested, as well as the residuals from the best fit trend surfaces. Associations between the results of this analysis and the observed change in shear strength were then rationalized.

### 2.6. Summary profiles of statistical profiles

Summary profiles were also calculated to visualize what the statistical profiles looked like for an entire plot. For each plot, all profiles of a given statistical descriptor were utilized to generate a median profile of the given

Table 2
Significant changes in slope-normal stratigraphic dimensions, including slab thickness, and the separation distance with its upper and lower segments

| | Separation distance | Lower segment of separation distance ($d'$) | Upper segment of separation distance ($d''$) | Slab thickness |
|---|---|---|---|---|
| Mean±S.D.$_{Plot\ 1}$ (mm) | 18.99±2.56 | 10.04±2.39 | 8.95±1.83 | 236.89±7.22 |
| Mean±S.D.$_{Plot\ 2}$ (mm) | 16.69±2.10 | 9.20±1.81 | 7.49±1.90 | 253.19±18.10 |
| ΔMean (mm) | −2.30 | −0.84 | −1.46 | 16.30 |
| ΔMean (%) | −12.11 | −8.41 | −16.28 | 6.88 |
| Median$_{Plot\ 1}$ (mm) | 18.96 | 10.24 | 9.04 | 236.89 |
| Median$_{Plot\ 2}$ (mm) | 16.54 | 9.34 | 7.26 | 253.19 |
| ΔMedian (mm) | −2.42 | −0.91 | −1.79 | 16.30 |
| ΔMedian (%) | −12.76 | −8.85 | −19.74 | 6.88 |
| *p*-value | <0.001 | <0.001 | 0.002 | <0.001 |
| *z*-score | 6.9 | 5.4 | 3.1 | −7.6 |

ΔMean and ΔMedian signify changes in mean and median thickness. *p*-value and *z*-score pertain to the non-parametric Mann–Whitney (Wilcoxon Rank-Sum) test ($n_{plot1}=83$, $n_{plot2}=128$).

descriptor. For example, for plot 1 a median profile of the 90th percentile profiles was calculated using all 83 of the 90th percentile statistical profiles obtained from plot 1. Summary profiles were then plotted together to visualize changes.

## 3. Results

### 3.1. Spatial analysis of stratigraphic dimensions and hardness

Spatial statistics of SMP-derived variables at plots 1 and 2 are listed in Table 1. At plot 1, very few variables possessed significant ($p \leq 0.05$) trend surfaces or positive spatial autocorrelation. Of the eleven significant trend surfaces at plot 1, eight describe substratum hardness characteristics (Table 1). Similarly, the lower transition and the substratum boundary possessed most of the spherical semivariance models at plot 1 (Table 1). The CoV at the substratum boundary possessed a significant ($p = 0.0019$) trend surface and pronounced positive autocorrelation. The separation distance at plot 1 also possessed both components of spatial structure.

At plot 2, all hardness variables and the CoV at all five stratigraphic positions possessed spatial structure in the form of significant trend surfaces, positive autocorrelation or, as was the case for most variables, a combination (Table 1). The majority of variables that did not possess positive spatial autocorrelation were those describing the central portion of the weak layer (Table 1). While the separation distance possessed no spatial patterns at plot 2, the slab thickness possessed both types of spatial structure (Table 1).

Between plots 1 and 2, a notable discrepancy existed between the dimensions of the semivariance models produced for hardness variables at the substratum boundary (Fig. 6). For statistical descriptors apart from the first quartile statistic, the range values increased, the partial sill values decreased, and the nugget values increased (Table 1, and Fig. 6). Hence, for these hardness variables at the substratum boundary, plot 2 possessed broader spatial variations, lower plot-scale variances, and a higher inherent "noise" or stochastic character (i.e. a higher nugget–sill ratio) (Fig. 6).

### 3.2. Significant changes in stratigraphic dimensions between plots 1 and 2

Between plots 1 and 2, the mean slope-normal separation distance decreased significantly ($p \leq 0.001$) from 19.0 mm to 16.7 mm, signifying a 12.1% decrease in mean thickness while the standard deviation decreased from 2.56 mm to 2.10 mm (Table 2 and Fig. 7a). The reduction in size is evident in both the upper and lower segments of the separation distance (Table 2). Snow profile observations also indicated that the weak layer thinned markedly in the 6 days between plots 1 and 2, 6 days apart, from 2 cm to 1 cm (estimated to the nearest centimeter), and that the maximum observed crystal size decreased from 15 mm to 8 mm.

Mean slope-normal slab thickness increased significantly ($p < 0.001$) from 23.7 cm to 25.3 cm between the two plots, 6 days apart (Table 2 and Fig. 7b). This increase of 1.6 cm coincided with a small snowstorm that occurred between observation days (see Landry, 2002 for a detailed description of the snowpack development).

### 3.3. Significant changes in stratigraphic hardness between plots 1 and 2

Significant ($p \leq 0.05$) changes in the non-parametric hardness variables at all five slope-normal stratigraphic

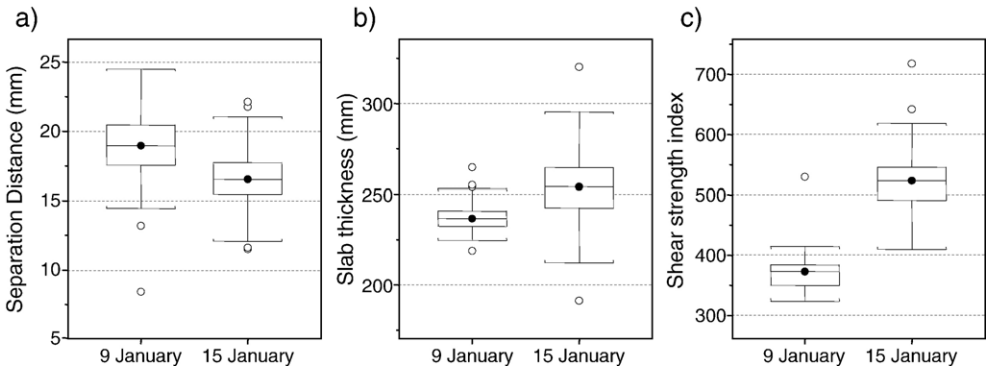


Fig. 7. Boxplots of selected variables showing significant changes between January 9th and 15th, including (a) the separation distance between the super- and substrata boundaries, (b) the slab thickness, and (c) the size-corrected shear strength index. Black circles = median, box ends = 1st and 3rd quartiles, whiskers = 1.5 * inter-quartile range, white circles = outliers.

Table 3
Significance of changes in SMP-derived hardness variables between plots 1 and 2, as tested using the non-parametric Mann–Whitney (Wilcoxon Rank-Sum) test ($n_{plot1}=83$, $n_{plot2}=128$)

| Variable | Plot 1 mean±S.D. | Plot 2 mean±S.D. | *p*-value | *z*-score | ΔMean | ΔMean (%) |
|---|---|---|---|---|---|---|
| *Superstratum boundary* | | | | | | |
| Max (*N*) | 0.2022±0.0599 | 0.2027±0.0723 | 0.881 | 0.2 | 0.0006 | 0.0028 |
| 98th (*N*) | 0.1615±0.0443 | 0.1566±0.0538 | 0.367 | 0.9 | −0.0049 | −0.0306 |
| 90th (*N*) | **0.1329±0.0339** | **0.1205±0.0337** | **0.034** | **2.1** | **−0.0124** | **−0.0933** |
| 75th (*N*) | **0.1139±0.0284** | **0.0989±0.0282** | **0.001** | **3.3** | **−0.0150** | **−0.1318** |
| Median (*N*) | **0.0967±0.0251** | **0.0799±0.0239** | **<0.001** | **4.6** | **−0.0168** | **−0.1739** |
| 25th (*N*) | **0.0809±0.0224** | **0.0628±0.0205** | **<0.001** | **5.5** | **−0.0181** | **−0.2238** |
| 10th (*N*) | **0.0683±0.0204** | **0.0500±0.0177** | **<0.001** | **6.3** | **−0.0184** | **−0.2687** |
| Min (*N*) | **0.0381±0.0161** | **0.0212±0.0129** | **<0.001** | **7.6** | **−0.0169** | **−0.4429** |
| CoV | **0.2649±0.0506** | **0.3551±0.0690** | **<0.001** | **9.3** | **0.0902** | **0.3406** |
| *Upper transition* | | | | | | |
| Max (*N*) | 0.1751±0.0692 | 0.1960±0.0819 | 0.089 | −1.7 | 0.0209 | 0.1192 |
| 98th (*N*) | 0.1303±0.0442 | 0.1360±0.0559 | 0.87 | −0.2 | 0.0057 | 0.0435 |
| 90th (*N*) | 0.0899±0.0280 | 0.0885±0.0288 | 0.739 | 0.3 | −0.0014 | −0.0160 |
| 75th (*N*) | 0.0665±0.0199 | 0.0617±0.0201 | 0.111 | 1.6 | −0.0047 | −0.0712 |
| Median (*N*) | **0.0463±0.0154** | **0.0390±0.0141** | **0.001** | **3.4** | **−0.0073** | **−0.1585** |
| 25th (*N*) | **0.0301±0.0120** | **0.0227±0.0095** | **<0.001** | **4.6** | **−0.0074** | **−0.2465** |
| 10th (*N*) | **0.0201±0.0098** | **0.0133±0.0077** | **<0.001** | **5.1** | **−0.0068** | **−0.3366** |
| Min (*N*) | **0.0003±0.0072** | **−0.0036±0.0077** | **<0.001** | **3.7** | **−0.0039** | **−13.9707** |
| CoV | **0.5813±0.1649** | **0.7213±0.1837** | **<0.001** | **5.4** | **0.1399** | **0.2407** |
| *Weak layer middle* | | | | | | |
| Max (*N*) | **0.1267±0.0580** | **0.1497±0.0618** | **0.002** | **−3** | **0.0229** | **0.1810** |
| 98th (*N*) | **0.0808±0.0380** | **0.0940±0.0430** | **0.012** | **−2.5** | **0.0131** | **0.1626** |
| 90th (*N*) | **0.0444±0.0202** | **0.0498±0.0218** | **0.046** | **−2** | **0.0053** | **0.1196** |
| 75th (*N*) | 0.0288±0.0142 | 0.0296±0.0130 | 0.277 | −1.1 | 0.0009 | 0.0299 |
| Median (*N*) | 0.0182±0.0104 | 0.0173±0.0079 | 0.64 | −0.5 | −0.0008 | −0.0462 |
| 25th (*N*) | 0.0109±0.0078 | 0.0097±0.0062 | 0.86 | 0.2 | −0.0012 | −0.1063 |
| 10th (*N*) | 0.0055±0.0065 | 0.0044±0.0057 | 0.767 | 0.3 | −0.0011 | −0.2023 |
| Min (*N*) | −0.0077±0.0061 | −0.0094±0.0071 | 0.234 | 1.2 | −0.0017 | 0.2145 |
| CoV | **0.9030±0.2499** | **1.0515±0.4372** | **0.046** | **2** | **0.1485** | **0.1645** |
| *Lower transition* | | | | | | |
| Max (*N*) | **0.1406±0.0502** | **0.1742±0.0588** | **<0.001** | **−4.7** | **0.0336** | **0.2393** |
| 98th (*N*) | **0.1017±0.0408** | **0.1176±0.0388** | **<0.001** | **−3.9** | **0.0159** | **0.1567** |
| 90th (*N*) | **0.0753±0.0325** | **0.0817±0.0294** | **0.018** | **−2.4** | **0.0064** | **0.0845** |
| 75th (*N*) | 0.0564±0.0259 | 0.0589±0.0235 | 0.18 | −1.3 | 0.0025 | 0.0452 |
| Median (*N*) | 0.0390±0.0195 | 0.0387±0.0172 | 0.846 | −0.2 | −0.0002 | −0.0061 |
| 25th (*N*) | 0.0256±0.0137 | 0.0238±0.0114 | 0.429 | 0.8 | −0.0018 | −0.0686 |
| 10th (*N*) | 0.0162±0.0097 | 0.0143±0.0081 | 0.388 | 0.9 | −0.0020 | −0.1208 |
| Min (*N*) | −0.0020±0.0067 | −0.0038±0.0078 | 0.152 | 1.4 | −0.0019 | 0.9453 |
| CoV | **0.5725±0.1055** | **0.6604±0.1381** | **<0.001** | **4.4** | **0.0879** | **0.1535** |
| *Substratum boundary* | | | | | | |
| Max (*N*) | **0.2083±0.0628** | **0.2357±0.0644** | **<0.0001** | **−3.8** | **0.0275** | **0.1318** |
| 98th (*N*) | **0.1677±0.0552** | **0.1828±0.0522** | **0.008** | **−2.7** | **0.0151** | **0.0901** |
| 90th (*N*) | 0.1385±0.0495 | 0.1473±0.0454 | 0.088 | −1.7 | 0.0088 | 0.0633 |
| 75th (*N*) | 0.1185±0.0453 | 0.1230±0.0413 | 0.312 | −1 | 0.0046 | 0.0385 |
| Median (*N*) | 0.0995±0.0404 | 0.1003±0.0363 | 0.801 | −0.3 | 0.0008 | 0.0085 |
| 25th (*N*) | 0.0795±0.0349 | 0.0780±0.0310 | 0.718 | 0.4 | −0.0016 | −0.0198 |
| 10th (*N*) | 0.0638±0.0295 | 0.0612±0.0266 | 0.383 | 0.9 | −0.0026 | −0.0413 |
| Min (*N*) | 0.0279±0.0205 | 0.0255±0.0191 | 0.274 | 1.1 | −0.0024 | −0.0864 |
| CoV | **0.3047±0.0489** | **0.3488±0.0645** | **<0.001** | **5.2** | **0.0441** | **0.1448** |

Variables exhibiting significant ($p$-value ≤ 0.05) changes in median values are listed in bold print. ΔMean signifies the change in mean hardness or the CoV of hardness.

positions are summarized in Table 3 and graphically depicted in Fig. 8. Fig. 9 depicts the plot summaries of the non-parametric statistical profiles. Two general trends are evident in the hardness characteristics. First, a significant increase in hardness is evident at the middle and lower stratigraphic positions in the variables describing the upper percentiles, including the 90th and 98th percentiles, and the maximum. Second, a significant decrease of hardness values occurred at the upper transition and superstratum positions, primarily in those variables describing the minimum and median hardness values. This finding corresponds with the snow profile observation: "slab softer…barely cohesive" (Landry, 2002, p. 246). The temperature gradient through the buried surface hoar layer was 8 °C $m^{-1}$ on January 9th (plot 1) and 16 °C $m^{-1}$ on January 15th (plot 2). Approximate temperature gradients through the slab were 16.5 °C $m^{-1}$ and 9 °C $m^{-1}$, respectively.

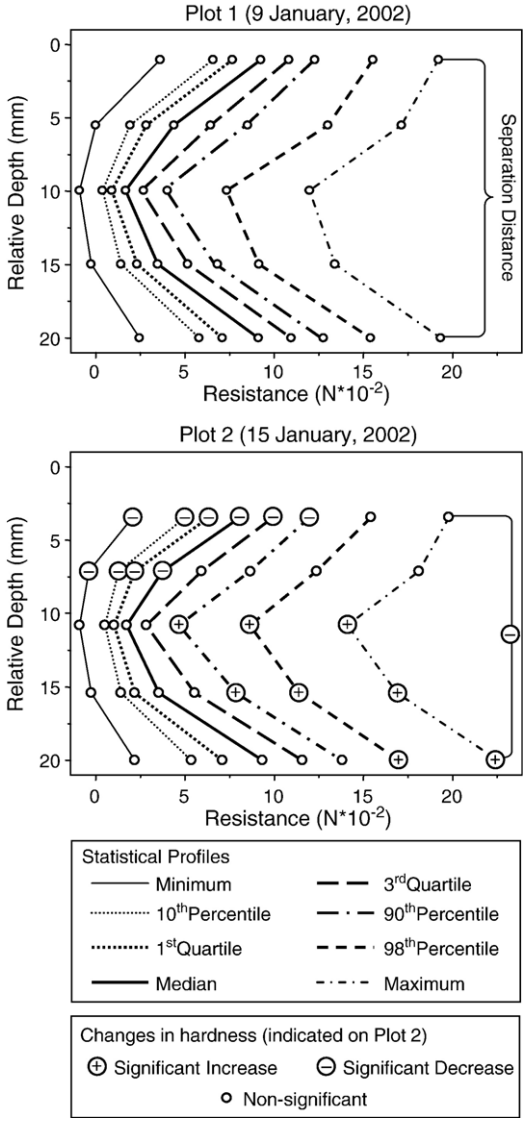


Fig. 8. Graphical summary of the changes in weak layer hardness, as described by non-parametric statistics. Significant ($p \leq 0.05$) changes in hardness are shown on plot 2, whereby +/− signs are used to describe significant increases or decreases in hardness.

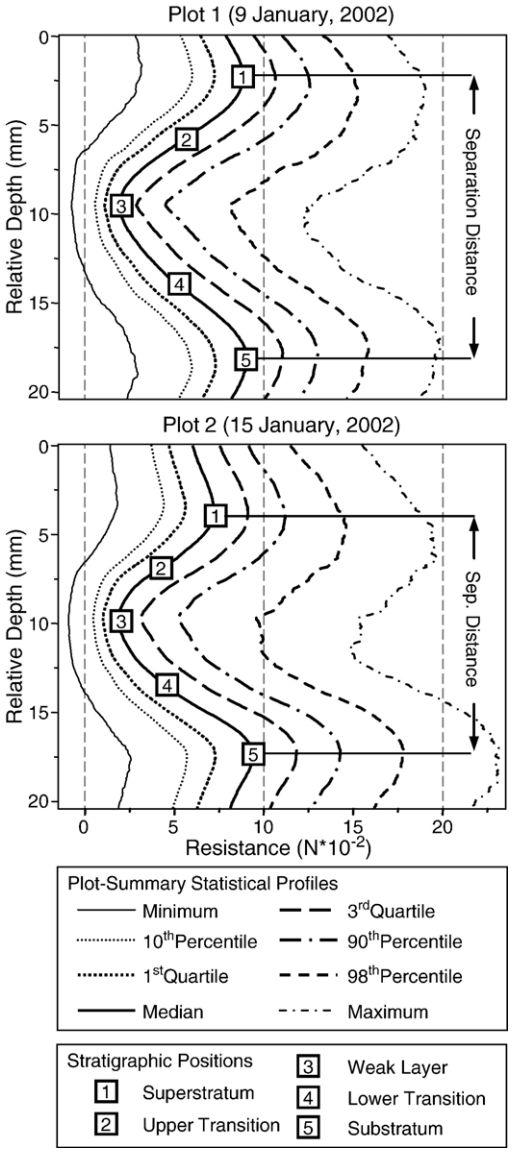


Fig. 9. Plot summaries of statistical profiles.

At both plots 1 and 2, the CoV of the resistance signal was greatest at the center of the weak layer and smallest at the super- and substrata boundaries (Table 3 and Fig. 10). There were significant ($p \leq 0.05$) increases in CoV at all five slope-normal stratigraphic positions, the least significant ($p = 0.046$) of which occurred at the weak

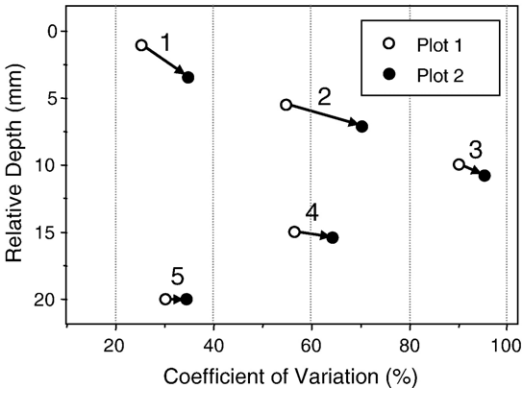


Fig. 10. At both plots the coefficient of variation (CoV) was greatest within the weak layer and smallest at the boundaries with the adjacent strata. Numbers indicate stratigraphic positions while arrows indicate relative change of CoV and stratigraphic position, relative to the substratum boundary position.

layer position, while highly significant ($p=0.001$) increases occurred at the remaining four positions.

### 3.4. Relationships between slab thickness and weak layer characteristics

Table 4 summarizes the regression results correlating slab thickness with the other SMP-derived variables. Only the results from regression tests using uncorrected values are listed, since their significance and explanatory values were slightly higher than those produced using the residuals from the best fit linear trend surfaces.

Plot 1 possessed few significant relationships, all with explanatory values less than 10% (Table 4). However, plot 2 possessed several highly significant ($p<0.001$) positive correlations between slab thickness and hardness of the super- and substrata boundaries. Explanatory values were highest at the substratum boundary, ranging from 13.4% to 33.2%.

Significant negative correlations were identified between slab thickness and CoV of hardness at plots 1 and 2. At plot 1, a small ($R^2=0.054$) but significant ($p=0.034$) inverse correlation existed between slab thickness and the CoV at the substratum boundary. At plot 2, this inverse relationship was highly significant ($p\leq 2\times 10^{-9}$) and explained 25.3% of the variation of the CoV. In addition, at plot 2 a significant ($p=0.017$) negative correlation existed between slab thickness and the CoV of hardness.

Slab thickness also possessed significant ($p=0.03$ and 0.0002, respectively) positive correlations with the separation distance at both plots, explaining about 5.7% and 10.9% of the variation in the separation distance at each plot respectively.

### 3.5. Overview of stability test results

Classical analysis of the stability test results indicated a significant ($p\leq 0.001$) increase of the mean size-corrected shear strength index values from 373.5 to 522.9 between plots 1 and 2, as well as an increase in the standard deviation from 37.1 to 54.8 (Fig. 7c). Stability test results are described and interpreted in detail by Birkeland and Landry (2002), Landry (2002), and Landry et al. (2004).

## 4. Discussion

### 4.1. Spatial characteristics of stratigraphic dimensions and hardness

The absence of spatial patterns from many of the SMP-derived variables at plot 1 suggests spatial uniformity at the scale of observation (Table 1). Hence, capturing the true spatial patterns of the natural phenomenon required a different sampling scheme possessing significantly different (smaller or larger) sample spacing. At plot 1, only the substratum boundary exhibited consistent spatial patterns.

In contrast, the extensive spatial structure at plot 2 reveals that the hardness characteristics at the super- and substrata boundaries are spatially autocorrelated and the weak layer center appears uniform (Table 1). The discrepancies between semivariance models of hardness characteristics at the substratum at plots 1 and 2 reveal three potentially temporal developments: (1) local patterns in hardness became broader (increased range values), (2) the plot-scale variability decreased (decreased partial sill values), and (3) the inherent noise increased (increased nugget) (Fig. 6). Recent modeling work suggests increased nugget–sill ratios in shear strength leads to increasing slope stability (Kronholm and Birkeland, 2005), so the temporal changes we observe might be a component of the slope stabilization process.

The semivariogram range for the weak layer hardness values was slightly longer than those found by Kronholm et al. (2004), but generally seem to be in agreement. An exact comparison is difficult, since Kronholm et al. (2004) excluded the weak layer's transitions and analyzed the mean of the log-transformed resistance signal.

For our results, the substrata boundary possessed consistent spatial characteristics, while large discrepancies are evident in the spatial characteristics of descriptors for other positions. For instance, the lower transition semivariogram range values at plot 2 vary from 4.5 m (for the median hardness) to 12.5 m (for the

Table 4
Regression results of correlations between slab thickness and weak layer hardness ($n_{plot1}=83$, $n_{plot2}=128$)

| Variable | Plot 1 | | | Plot 2 | | |
|---|---|---|---|---|---|---|
| | *p*-value | $R^2$ | Coeff. | *p*-value | $R^2$ | Coeff. |
| *Stratigraphic dimensions* | | | | | | |
| Separation distance (mm) | **0.0299** | **0.0569** | **0.0846** | **0.0002** | **0.1088** | **0.0385** |
| Upper segment (mm) | **0.0377** | **0.0522** | **0.0578** | **0.0041** | **0.0646** | **0.0266** |
| Lower segment (mm) | 0.4677 | 0.0065 | 0.0268 | 0.1730 | 0.0149 | 0.0119 |
| *Superstratum boundary hardness* | | | | | | |
| Max (*N*) | 0.0937 | 0.0343 | 0.0015 | **0.0053** | **0.0610** | **0.0010** |
| 98th (*N*) | **0.0150** | **0.0709** | **0.0016** | **0.0006** | **0.0913** | **0.0009** |
| 90th (*N*) | **0.0098** | **0.0795** | **0.0013** | **3.8e−05** | **0.1285** | **0.0007** |
| 75th (*N*) | **0.0243** | **0.0610** | **0.0010** | **1.2e−05** | **0.1440** | **0.0006** |
| Median (*N*) | **0.0257** | **0.0600** | **0.0009** | **2.7e−06** | **0.1633** | **0.0005** |
| 25th (*N*) | **0.0282** | **0.0581** | **0.0007** | **1.0e−06** | **0.1758** | **0.0005** |
| 10th (*N*) | **0.0387** | **0.0517** | **0.0006** | **7.3e−07** | **0.1801** | **0.0004** |
| Min (*N*) | **0.0040** | **0.0978** | **0.0007** | **0.0008** | **0.0864** | **0.0002** |
| CoV | 0.5452 | 0.0045 | −0.0005 | **0.0173** | **0.0448** | **−0.0008** |
| *Upper transition hardness* | | | | | | |
| Max (*N*) | 0.3717 | 0.0099 | 0.0010 | 0.1599 | 0.0159 | 0.0006 |
| 98th (*N*) | 0.1355 | 0.0273 | 0.0010 | **0.0319** | **0.0366** | **0.0006** |
| 90th (*N*) | **0.0172** | **0.0681** | **0.0010** | **0.0227** | **0.0412** | **0.0003** |
| 75th (*N*) | 0.1163 | 0.0302 | 0.0005 | **0.0039** | **0.0651** | **0.0003** |
| Median (*N*) | 0.2109 | 0.0193 | 0.0003 | **0.0013** | **0.0806** | **0.0002** |
| 25th (*N*) | 0.1606 | 0.0242 | 0.0003 | **0.0009** | **0.0851** | **0.0002** |
| 10th (*N*) | 0.1386 | 0.0269 | 0.0002 | **0.0026** | **0.0707** | **0.0001** |
| Min (*N*) | **0.0181** | **0.0670** | **0.0003** | 0.6652 | 0.0015 | 1.7e−05 |
| CoV | 0.9853 | 4.2e−06 | 4.7e−05 | 0.4367 | 0.0049 | −0.0007 |
| *Weak layer middle hardness* | | | | | | |
| Max (*N*) | 0.4051 | 0.0086 | −0.0007 | 0.8707 | 0.0002 | −5.0e−05 |
| 98th (*N*) | 0.9142 | 0.0001 | −0.0001 | 0.8326 | 0.0004 | −4.5e−05 |
| 90th (*N*) | 0.7031 | 0.0018 | −0.0001 | 0.7455 | 0.0009 | 3.5e−05 |
| 75th (*N*) | 0.5907 | 0.0036 | −0.0001 | 0.6471 | 0.0017 | 3.0e−05 |
| Median (*N*) | 0.6055 | 0.0033 | −0.0001 | 0.4327 | 0.0050 | 3.1e−05 |
| 25th (*N*) | 0.6716 | 0.0022 | −0.0001 | 0.9696 | 0.0000 | 1.2e−06 |
| 10th (*N*) | 0.6967 | 0.0019 | −3.9e−05 | 0.5779 | 0.0025 | −1.6e−05 |
| Min (*N*) | 0.3850 | 0.0093 | −0.0001 | 0.0600 | 0.0282 | −0.0001 |
| CoV | 0.9675 | 2.1e−05 | −0.0002 | 0.5935 | 0.0023 | −0.0012 |
| *Lower transition hardness* | | | | | | |
| Max (*N*) | 0.6049 | 0.0033 | 0.0004 | 0.0594 | 0.0284 | 0.0005 |
| 98th (*N*) | 0.6595 | 0.0024 | 0.0003 | **0.0012** | **0.0818** | **0.0006** |
| 90th (*N*) | 0.8794 | 0.0003 | 0.0001 | **0.0006** | **0.0921** | **0.0005** |
| 75th (*N*) | 0.7249 | 0.0015 | 0.0001 | **0.0009** | **0.0850** | **0.0004** |
| Median (*N*) | 0.7103 | 0.0017 | 0.0001 | **0.0038** | **0.0657** | **0.0002** |
| 25th (*N*) | 0.8316 | 0.0006 | 4.5e−05 | **0.0283** | **0.0382** | **0.0001** |
| 10th (*N*) | 0.9536 | 4.2e−05 | 8.7e−06 | 0.1092 | 0.0206 | 0.0001 |
| Min (*N*) | 0.8159 | 0.0007 | 2.4e−05 | 0.4779 | 0.0041 | −2.7e−05 |
| CoV | 0.4232 | 0.0079 | −0.0013 | 0.6626 | 0.0015 | −0.0003 |
| *Substratum boundary hardness* | | | | | | |
| Max (*N*) | 0.1265 | 0.0286 | 0.0015 | **2.6e−05** | **0.1336** | **0.0013** |
| 98th (*N*) | 0.0667 | 0.0409 | 0.0015 | **1.9e−08** | **0.2258** | **0.0014** |
| 90th (*N*) | 0.0695 | 0.0401 | 0.0014 | **3.4e−10** | **0.2733** | **0.0013** |
| 75th (*N*) | 0.0787 | 0.0377 | 0.0012 | **6.6e−11** | **0.2918** | **0.0012** |
| Median (*N*) | 0.0701 | 0.0399 | 0.0011 | **3.6e−11** | **0.2987** | **0.0011** |

Table 4 (*continued*)

| Variable | Plot 1 | | | Plot 2 | | |
|---|---|---|---|---|---|---|
| | *p*-value | $R^2$ | Coeff. | *p*-value | $R^2$ | Coeff. |
| *Substratum boundary hardness* | | | | | | |
| 25th (*N*) | 0.0761 | 0.0383 | 0.0009 | **1.7e−12** | **0.3317** | **0.0010** |
| 10th (*N*) | 0.0640 | 0.0417 | 0.0008 | **2.0e−12** | **0.3303** | **0.0008** |
| Min (*N*) | **0.0375** | **0.0523** | **0.0006** | **1.1e−08** | **0.2325** | **0.0005** |
| CoV | **0.0344** | **0.0541** | **−0.0016** | **2.0e−09** | **0.2526** | **−0.0018** |

Significant ($p \leq 0.05$) correlations are listed in bold.

first quartile of hardness); a physical interpretation of this is difficult. The semivariograms for these variables show the spherical model (calculated using the weighted least squares function) "jumped" to a smaller range when the semivariance at short lag distances changed only slightly in the empirical variogram. This suggests using a more robust semivariogram model function would reduce the variation in the observed spatial patterns at a given stratigraphic position. Taking these limitations into account, the most important results of the spatial analysis are the general trends, the presence or absence of structure, and the typical structure(s) present at a given stratigraphic position (such as the substratum boundary).

### 4.2. Temporal associations between stratigraphic characteristics and weak layer strengthening

The tests for significant changes in stratigraphic dimensions and hardness characteristics of the weak layer revealed four interesting developments that coincided with the observed strengthening of the weak layer. First, the 12.1% decrease of the SMP-derived separation distance supports previous research that weak layer strengthening is accompanied by weak layer thinning (Table 2) (Davis et al., 1996; Jamieson and Schweizer, 2000). The results support the conceptual model proposed by Jamieson and Schweizer (2000) that the strengthening of buried surface layers is in part due to surface hoar penetration of the substratum, which would cause the total layer thickness to decrease. As described by Davis et al. (1998) and Jamieson and Schweizer (2000), umbrella-like surface hoar crystals possess larger contact areas with the superstratum than with the substratum. Hence, it is likely that the upper boundary would be better preserved, while the lower boundary would penetrate into the substratum due to the overburden. Another possible cause for weak layer thinning could be a slow shear strain due to the shear stress within the weak layer, which would cause the crystals to rotate down slope from their original orientation. However, in this study no observable change in the crystal orientation was noted.

Second, the increase in hardness at the lower transition and substratum boundary coincided with the increase in shear strength, supporting previous research that identified the lower boundary of the weak layer as the critical location for strengthening (Table 3) (Davis et al., 1996, 1998; Jamieson and Schweizer, 2000). Evidently, despite the large temperature gradients, bond strengthening or densification occurred. This observation conforms to the conceptual model proposed by Jamieson and Schweizer (2000) that due to hoar crystal penetration into the substratum, more surface area is made available for bonding with the substratum.

Third, the decrease in hardness observed at the upper transition and superstratum boundary most likely was due to faceting in the upper portion of the snowpack (Table 3). Faceting was possible due to large temperature gradients present within the weak layer and the slab during the sampling period. The weaker resistance values imply that grain bonds became weaker or less dense, likely due to faceting. Since the shear strength did not decrease, but actually increased between plots 1 and 2, it appears that the hardness of upper transition and the superstratum boundary did not govern changes in shear strength.

Fourth, the CoV of hardness revealed two interesting textural characteristics of the superstratum–weak layer–substratum complex. The surface hoar possessed much higher CoV values than the adjacent boundaries, since the surface hoar produced smaller mean resistance values and are highly heterogeneous. Viewed temporally, it is evident that the CoV of hardness increased, suggesting that the weak layer structure became more variable at the scale of the moving window statistical operations (Table 3). This may have been due to the degradation of surface hoar as it aged.

### 4.3. Relationships between slab thickness and stratigraphic characteristics

Slab thickness appears to influence three stratigraphic characteristics (Table 4). First, the positive correlations between slab thickness and the hardness of the super- and substrata boundaries provide evidence that

slab thickness positively influences the hardness of weak layer boundaries with adjacent strata. Assuming the slope-normal slab thickness is a proxy of the slope-normal load, it appears that, on a given slope at a given time, harder weak layer boundaries develop under greater loads. This relationship was stronger at plot 2 than at plot 1, suggesting that, the relationship became stronger with time, perhaps due to the small increase in overburden. Furthermore, the central portion of the weak layer was not affected by differences in slab thickness at either plot. This discrepancy is intuitive, since the boundaries of the surface hoar layer contact the adjacent strata and the central portion does not. Conversely, it would be counterintuitive if the central portion of the surface hoar layer would become harder under greater loads (temporally or spatially) without the boundaries hardening as well.

Second, the negative correlations identified at plots 1 and 2 between slab thickness and the CoV of hardness at the super- and substrata boundaries suggest that, at a given point in time, the hardness of the weak layer boundaries is less variable where the slab is thicker. Third, the weak positive relationships between slab thickness and the separation distance are counterintuitive, suggesting that at a given point in time, the weak layer was thicker where the slab was thicker. One possible cause would be that the SMP was not held perfectly perpendicular to the slope, thereby coupling thicker slab measurements with thicker weak layer measurements. The low explanatory values however show that most of the variation in slab thickness and the separation distance was not related.

### *4.4. Interpretation of weak layer delineation technique*

The concurrence of the significant decrease in the slope-normal separation distance and the field observations between plots 1 and 2 suggests that this stratigraphic delineation technique is picking up real stratigraphic features. Interestingly, two discrepancies can be identified between these findings and the weak layer thickness results calculated by Birkeland et al. (2004). First, Birkeland et al. (2004) found no significant weak layer thinning. A possible explanation for this discrepancy is differences in weak layer delineation criteria. Using manual delineation, the weak layer was defined as the segment of the resistance signal between the upper and lower transitions (excluding the transitions) (Fig. 1d). Hence, the thinning observed in our results must be occurring in the transition zones.

Second, the mean separation distances of 19.0 mm and 16.7 mm for plots 1 and 2 was markedly larger than the weak layer thickness of approximately 8 mm calculated by Birkeland et al. (2004). This discrepancy can be logically attributed to physical properties of the snowpack and the SMP geometry (Fig. 1). This can be best explained if we assume a hypothetical snowpack where the super- and substrata are homogenous layers and the weak layer is a void space, with acute transitions with the adjacent strata (Fig. 1b). The SMP would record a weak (void) layer bounded by two transition zones, each the length of the sensor tip (with quadratic decreasing or increasing form) (Fig. 1b). In this example, it is clear that the actual weak layer thickness is equal to the sum of the upper transition and the apparent weak layer segment. While Birkeland et al. (2004) delineated the weak layer as the signal segment between transitions, we included both transitions to obtain the hardness maximums at the boundaries with the adjacent strata. Hence, by adding the sensor head length of 4.3 mm to the Birkeland et al. (2004) results (Fig. 1c) and subtracting the sensor head length of 4.3 mm from our separation distance (Fig. 1d), the two studies have quite comparable weak layer dimensions (12.3 mm for Birkeland et al. (2004) and 14.7 mm and 12.4 mm for this study).

## 5. Conclusions

The moving window statistical operations developed and employed in this study enabled stratigraphic dimension and hardness characteristics of a surface hoar weak layer to be quantified. Our main findings are that: (1) differences between the stratigraphic dimensions calculated using this and the previously used delineation technique can be accounted for, (2) the hardness of the substratum boundary possessed pronounced spatial structure which developed in a fashion consistent with recent spatial models of slope stabilization process, (3) weak layer thinning and hardening of the weak layer and its boundary with the substratum coincided with observed weak layer strengthening, (4) slab thickness positively affected the hardness of the weak layer boundaries and inversely affected its hardness variation.

Our results quantitatively support previous research that examined weak layer strengthening characteristics (Davis et al., 1996, 1998; Jamieson and Schweizer, 2000). An important component of this work is the application of moving window statistical operations to detect the strengthening process using the SMP. Future work will further automate this analysis technique and will utilize additional data to see if the patterns we observed repeat for other surface hoar layers. If they do,

the SMP might prove to be a valuable tool for monitoring the strengthening of surface hoar weak layers.

## Acknowledgements

We are indebted to Chris Landry for the extensive stability and snow profile observations that he conducted at Lionhead in January of 2002 and has made available to this research group for further analysis. Dr. John Borkowski of the Department of Mathematical Sciences at Montana State University provided useful input on developing statistical methodologies. Comments by two anonymous reviewers greatly improved the clarity and focus of our paper. This research has been partially funded through the National Science Foundation Geography and Regional Science Program (BCS-0240310).

## References

Bader, H.P., Haefeli, R., Bucher, E., Neher, J., Eckel, O., Thams, C., 1939. Der Schnee und seine Metamorphose. Beitraege zur Geologie der Schweiz. Geotechnische Serie, Hydrologie Lieferung, vol. 3. Kümmerly & Frey, Zürich.

Birkeland, K., Landry, C., 2002. Changes in spatial patterns of snow stability through time. Proceedings of the 2002 International Snow Science Workshop, Penticton, British Colombia, Canada, pp. 482–490. http://www.fsavalanche.org/NAC/techPages/articles/02_ISSW_spatial_var_time.pdf.

Birkeland, K., Kronholm, K., Schneebeli, M., Pielmeier, C., 2004. Temporal changes in the shear strength and hardness of a buried surface hoar layer. Ann. Glaciol. 38, 223–228.

Blöschl, G., 1999. Scaling issues in snow hydrology. Hydrol. process. 13, 2149–2175.

Bradley, C.C., 1968. The resistogram and the compressive strength of snow. J. Glaciol. 7 (51), 499–506.

Cressie, N.A.C., 1993. Statistics for spatial data, Wiley Series in Probability and Mathematical Statistics, Revised edition. John Wiley & Sons, New York.

Davis, R., Jamieson, B., Hughes, J., Johnston, C., 1996. Observations on buried surface hoar—persistent failure planes for slab avalanches in British Columbia, Canada. Proceedings of the 1996 International Snow Science Workshop, Banff, Alberta, Canada, pp. 81–85.

Davis, R., Jamieson, B., Johnston, C., 1998. Observations on buried surface hoar in British Columbia, Canada: section analyses of layer evolution. Proceedings of the 1998 International Snow Science Workshop, Sunriver, Oregon, USA, pp. 86–92.

DeQuervain, M., Meister, R., 1987. 50 years of snow profiles on the Weissfluhjoch and relations to the surrounding avalanche activity (1936/37–1985/86). In: Salm, B., Gubler, H. (Eds.), Avalanche Formation, Movement and Effects. International Association of Hydrological Sciences, Publication No. 162, pp. 161–181.

Dowd, T., Brown, R.L., 1986. A new instrument for determining strength profiles in snowcover. J. Glaciol. 32 (111), 299–301.

Fotheringham, A.S., Brunsdon, Ch., Charlton, M., 2002. Quantitative Geography: Perspectives on Spatial Data Analysis. Sage Publications Ltd., London, p. 270.

Jamieson, J.B., Schweizer, J., 2000. Texture and strength changes of buried surface-hoar layers with implications for dry snow-slab avalanche release. J. Glaciol. 46 (152), 151–160.

Johnson, J., Schneebeli, M., 1999. Characterizing the microstructural and micromechanical properties of snow. Cold Reg. Sci. Technol. 30 (1–3), 91–100.

Kronholm, K., Birkeland, K.W., 2005. Integrating spatial patterns into a snow avalanche cellular automata model. Geophys. Res. Lett. 32, L19504.

Kronholm, K., Schneebeli, M., Schweizer, J., 2004. Spatial variability of micro-penetration resistance in snow layers on a small slope. Ann. Glaciol. 38, 202–208.

Landry, C.C., 2002. Spatial variation in snow stability on uniform slopes: implications for extrapolation to surrounding terrain. M.S. Thesis, Department of Earth Sciences, Montana State University, Bozeman, Montana, USA. http://www.fsavalanche.org/NAC/techPages/theses/landry.pdf.

Landry, C.C., Borkowski, J., Brown, R.L., 2001. Quantified loaded column stability test: mechanics, procedure, sample-size selection, and trials. Cold Reg. Sci. Technol. 33 (2–3), 103–121.

Landry, C.C., Birkeland, K., Hansen, K., Borkowski, J., Brown, R., Aspinall, R., 2002. Snow stability on uniform slopes: implications for avalanche forecasting. Proceedings of the 2002 International Snow Science Workshop, Penticton, British Colombia, Canada, pp. 532–539.

Landry, C., Birkeland, K., Hansen, K., Borkowski, J., Brown, R., Aspinall, R., 2004. Variations in snow strength and stability on uniform slopes. Cold Reg. Sci. Technol. 39 (2–3), 205–218.

Louchet, F., 2001. Creep instability of the weak layer and natural slab avalanche triggerings. Cold Reg. Sci. Technol. 33 (2–3), 141–146.

Mackenzie, R., Payten, W., 2002. A portable, variable-speed, penetrometer for snow pit evaluation. Proceedings of the 2002 International Snow Science Workshop, Penticton, British Colombia, Canada, pp. 294–300.

O'Sullivan, D., Unwin, D.J., 2002. Geographic Information Analysis. John Wiley & Sons, Inc., Hoboken, New Jersey.

Pielmeier, C., Schneebeli, M., 2000. Measuring snow profiles with high-resolution: interpretation of the force-distance signal from a snow micro penetrometer. Proceedings of the 2000 International Snow Science Workshop, Big Sky, Montana, USA, pp. 215–222.

Pielmeier, C., Schneebeli, M., 2003. Snow stratigraphy measured by snow hardness and compared to surface section images. Cold Reg. Sci. Technol. 37 (3), 393–405.

Pielmeier, C., Schneebeli, M., Stucki, T., 2001. Snow texture: a comparison of empirical versus simulated texture index for alpine snow. Ann. Glaciol. 32, 7–13.

Schneebeli, M., 1999. High resolution penetrometry in the high-porosity material snow. Proceedings of the International Workshop on Penetrometry in the Solar System, Graz, Verlag der Österreichischen Akademie der Wissenschaften Wien, pp. 61–72.

Schneebeli, M., Johnson, J.B., 1998. A constant-speed penetrometer for high-resolution snow stratigraphy. Ann. Glaciol. 26, 107–111.

Schneebeli, M., Pielmeier, C., Johnson, J., 1999. Measuring snow microstructure and hardness using a high resolution penetrometer. Cold Reg. Sci. Technol. 30 (1–3), 101–114.

Schweizer, J., Wiesinger, T., 2003. Snow profile interpretation for stability evaluation. Cold Reg. Sci. Technol. 33 (2–3), 179–188.